EUROFUSION CP(15)05/98

M. Sertoli et al.

Interplay Between Central ECRH and MHD in Mitigating Tungsten Accumulation in ASDEX Upgrade

(22nd June 2015 – 26th June 2015)
Lisbon, Portugal

This work has been carried out within the framework of the EUROfusion Consortium and has received funding from the Euratom research and training programme 2014-2018 under grant agreement No 633053. The views and opinions expressed herein do not necessarily reflect those of the European Commission.

“This document is intended for publication in the open literature. It is made available on the clear understanding that it may not be further circulated and extracts or references may not be published prior to publication of the original when applicable, or without the consent of the Publications Officer, EUROfusion Programme Management Unit, Culham Science Centre, Abingdon, Oxon, OX14 3DB, UK or e-mail Publications.Officer@euro-fusion.org”.

“Enquiries about Copyright and reproduction should be addressed to the Publications Officer, EUROfusion Programme Management Unit, Culham Science Centre, Abingdon, Oxon, OX14 3DB, UK or e-mail Publications.Officer@euro-fusion.org”.

The contents of this preprint and all other EUROfusion Preprints, Reports and Conference Papers are available to view online free at http://www.euro-fusionscipub.org. This site has full search facilities and e-mail alert options. In the JET specific papers the diagrams contained within the PDFs on this site are hyperlinked.

Interplay between central ECRH and MHD in mitigating tungsten accumulation in ASDEX Upgrade

M. Sertoli[1], J. M. Garcia-Regaña[1,2], T. Odstrčil[1], C. Angioni[1], H. Smith[3], Y. Turkin[3], W. A. Cooper[4], A. de Bustos[5], D. Vezinet[1], the ASDEX Upgrade team and the EUROfusion MST1 Team*

[1] *Max-Planck-Institut für Plasmaphysik, D-85748 Garching, Germany*, [2] *EUROfusion PMU Garching, Boltzmannstrasse 1, D-85748, Garching, Germany*, [3] *Max-Planck-Institut für Plasmaphysik, 17491 Greifswald, Germany*, [4] *École Polytechnique Fédérale de Lausanne (EPFL, CRPP), 1015 Lausanne, Switzerland*, [5] *Departamento de Física, Universidad Carlos III, Leganés 28911, Madrid, Spain*, * *See http://www.euro-fusionscipub.org/mst1*

In tokamaks with reactor relevant high-Z plasma facing components (PFCs), the control of impurity accumulation in the plasma centre is of major importance to avoid performance degradation and the possible disruptive termination of the discharges due to excessive radiative power losses. At ASDEX Upgrade (AUG), whose first wall is fully covered with tungsten (W), the application of small amounts of electron cyclotron resonance heating (ECRH) has been found to be effective in mitigating central W accumulation which otherwise occurred in discharges where neutral beam (NBI) was used as sole auxiliary heating. The mitigation occurs only if the ECRH is deposited sufficiently central (typically inside the $q = 1$ surface) and usually in the presence of saturated $(m,n) = (1,1)$ MHD activity in-between sawtooth crashes. The interplay between ECRH and saturated $(1,1)$ modes in the mitigation of W accumulation is still not understood. Due to the helical equilibrium arising in the presence of the $(1,1)$ mode, typical experimental and theoretical methods employing 1D flux-surface-averaged quantities are not suited for the investigation of the processes in action. New experimental methods have been developed enabling a mode-resolved 2D measurement of the intrinsic W density by combining SXR tomographic reconstructions [1] with 2D rotation-tomography of the 1D electron cyclotron emission (ECE) electron temperature measurements [2]. These methods are here applied to a typical AUG H-mode discharge and the results compared with theoretical estimates evaluated with the coupled neoclassical and gyro-kinetic codes GKW [3] and NEO [4] (see [5] for details on the coupling method).

The plasma emission detected by the soft X-ray (SXR) diagnostic in most AUG discharges is dominated by W, typically accounting for 80% of the total emission in the plasma centre. In such cases, the tungsten density n_W can be evaluated from the experimental SXR emissivity ε_{exp}^{SXR} through the following equation:

$$n_W^{SXR}(\mathbf{r};t) \propto \varepsilon_{exp}^{SXR}(\mathbf{r};t) \,/\, [n_e(\mathbf{r};t)\, L_W^{SXR}(\mathbf{r},t)] \qquad (1)$$

where n_e is the electron density and L_W^{SXR} the radiation loss parameter (also called *cooling factor*) filtered according to the SXR diagnostic filter function (photon energy range $\sim 1-20$ keV at AUG) calculated assuming local ionization equilibrium. All quantities in equation (1) are defined in the three-dimensional space $\mathbf{r}$ of the tokamak and are a function of time. In the presence of a 3D helical equilibrium due to macroscopic MHD activity, equation (1) has to be solved at least on a 2D poloidal cross-section to resolve the various quantities on the non-axisymmetric equilibrium. This requires mode-resolved 2D maps of the SXR emissivity (tomographic reconstructions) and of the electron density for direct introduction in equation (1), as well as of the electron temperature for the calculation of the radiation loss parameter L_W^{SXR}. In this contribution, the 2D mode-resolved T_e maps have been evaluated following [2], while the n_e perturbation has been neglected and only the mode-averaged profiles have been used. The latter assumption is reasonable since the n_e profiles in the analysed experiment are relatively flat (see figure 2). Refer to [6, 7] for an in-depth explanation of the combined data analysis of SXR tomography and the 2D mode-resolved T_e maps for the correct application of equation (1).

The example reported is that of a standard AUG lower-single-null H-mode discharge (# 31114) with $I_p = 1$ MA, $B_t = -2.5$ T, $P_{NBI} = 7.5$ MW and $P_{ECRH} = 1.4$ MW. The ECRH power is equally distributed over two gyrotrons, the first one depositing at $\rho^H \sim 0.2$, the second one adjusted for co-ECCD for sawtooth control (deposition position scanned in range $\rho^{CD} \sim 0.2 \rightarrow 0.6$, leading to a total driven current $I_{CD} \sim 11 \rightarrow 5$ kA). In the analysed time range, the CD gyrotron sits close to the inversion radius $\rho_{inv} \sim 0.4$ (see figure 2). The radial coordinate $\rho = \sqrt{(\psi - \psi_a)/(\psi_s - \psi_a)}$ is the normalised poloidal flux radius, where ψ is the poloidal flux and the indices s and a refer to the separatrix and the magnetic axis.

The flux-surface-averaged W density has been first of all evaluated applying equation (1) with $\mathbf{r} = \rho$ and averaging all quantities over 10 ms (corresponding to ~ 100 mode rotations) to obtain mode-averaged profiles. The SXR emissivity has been evaluated through 1D Abel inversion of cameras I and J . As performed in [6] the obtained n_W^{SXR} has been cross-calibrated using the independent W concentration measurement of the grazing incidence spectrometer (GIW). The time evolution of the post-calibration W density at three radial positions is shown in figure 1a. The evolution of the simulated GIW measurement $c_{W,l}^{SXR}$ (post-calibration, dashed black line with red error bars in figure 1b) matches very well that of the spectrometer measurement (thick continuous black line). The sawtooth crashes, clearly visible in the time evolution of the W density and GIW measurement, are *inverted*, i.e. the profiles are hollow before the crash occurs, flattening inside $\rho \leq 0.4$ at the crash (already shown in the past for AUG in [8]). Strong MHD activity lasting more than half of the sawtooth period is visible in the spectrogram of a magnetic coil positioned at the LFS mid-plane (figure 1c). Both modes at frequencies ~ 10 kHz and ~ 13 kHz are $(1,1)$ modes (mode numbers evaluated from SXR and magnetic coils).

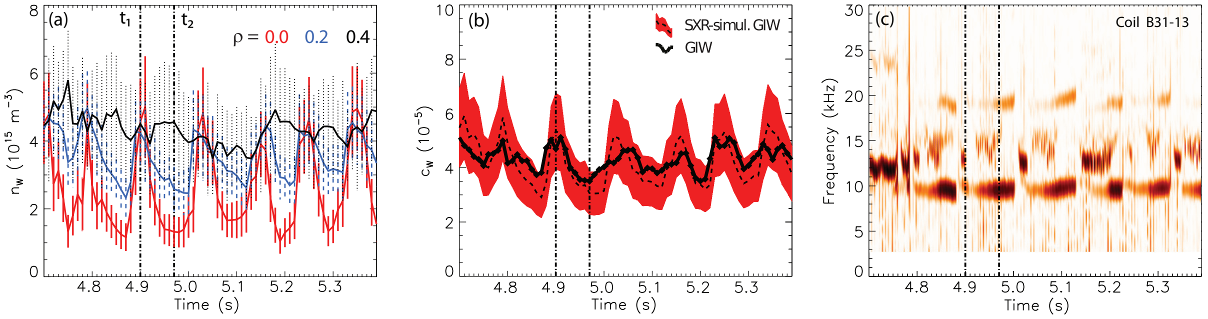

Figure 1: Time evolution of: (a) W density from SXR (all at three different radii); (b) comparison of simulated and experimental most central GIW measurement, (c) spectrogram of magnetic coil $B31-13$.

The evolution of the profiles during one sawtooth cycle are analysed more in detail for two time-points: $t_1 = 4.90$ - shortly after the sawtooth crash; $t_2 = 4.97$ - at mode saturation, shortly before the next crash occurs (shown as dashed black vertical lines in figure 1). The profiles of T_e, n_e, T_i and v_{rot} show minor changes (figure 2a-d), while major excursions are visible in the SXR emissivity (e), reflected in the W density profiles (figure 2f). Just after the crash, n_W is flat inside $\rho_{inv} \sim 0.4$ and develops a deep and wide hollowness before the next crash occurs. This behaviour is detected by the GIW spectrometer as well, despite its averaging over large radial domains (full circles and triangles in figure 2f). Modelling the flux-surface-averaged W density profiles with the coupled codes GKW and NEO including both neoclassical and turbulent effects as well as the effects of toroidal rotation, neither the peaking for $\rho > 0.4$ nor the hollowness inside this radius are reproduced (red diamonds in figure 2f, rescaled to the experimental value at $\rho = 0.7$). Nonetheless the order of magnitude is compatible with experiment, while if turbulent effects are excluded and only the neoclassical contributions accounted for, the W density in the centre increases by two orders of magnitude. Since the sawtooth crash is not modelled, these results are shown for t_2 only.

For best comparison with the 1D profiles, the 2D mode-resolved maps have been evaluated close to the same time-points. Figure 3a shows the time evolution of the 2D T_e maps (and its isothermal contours) at the start of the sawtooth cycle (labelled $At \sim t_1$) and at four time-points

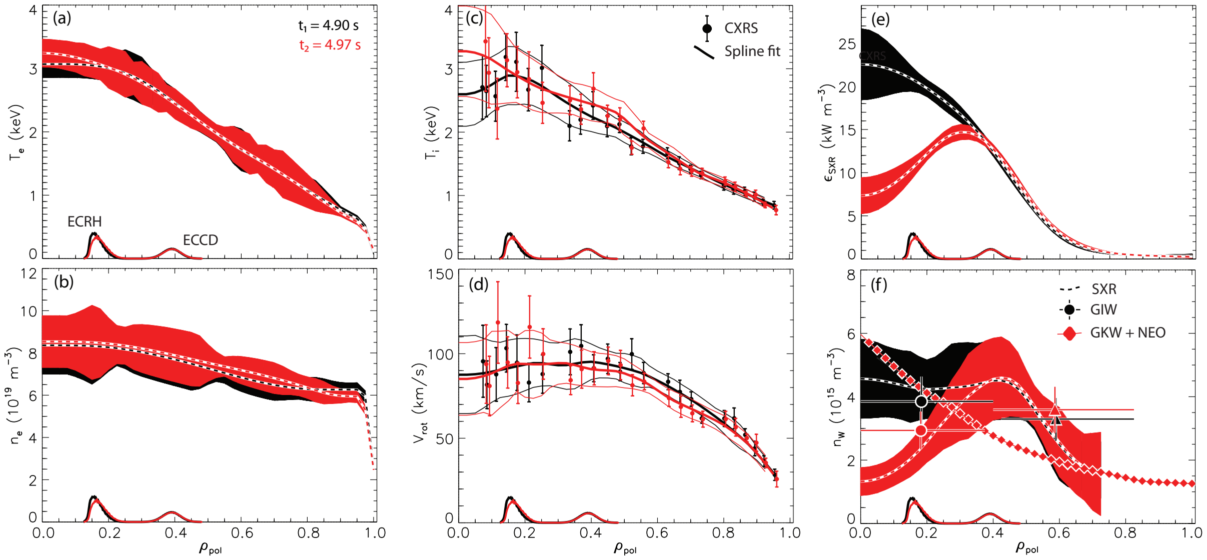

Figure 2: Profiles of (a) T_e, (b) n_e, (c) T_i, (d) v_{rot}, (e) ε_{exp}^{SXR} emissivity and (f) n_W^{SXR} compared to the measurements of the GIW spectrometer (full circles and triangles) and theoretical estimate using GKW + NEO (diamonds, rescaled to the experiment at $\rho = 0.7$) for two time-points (vertical lines in figure 1).

close to t_2 (labelled *Close to* t_2), the latter four occurring within a 43 μs time window (i.e. approximately half mode rotation). Also shown are the deposition position and the inversion radius (see labels) as well as the magnetic axis from the equilibrium reconstruction (black diamond).

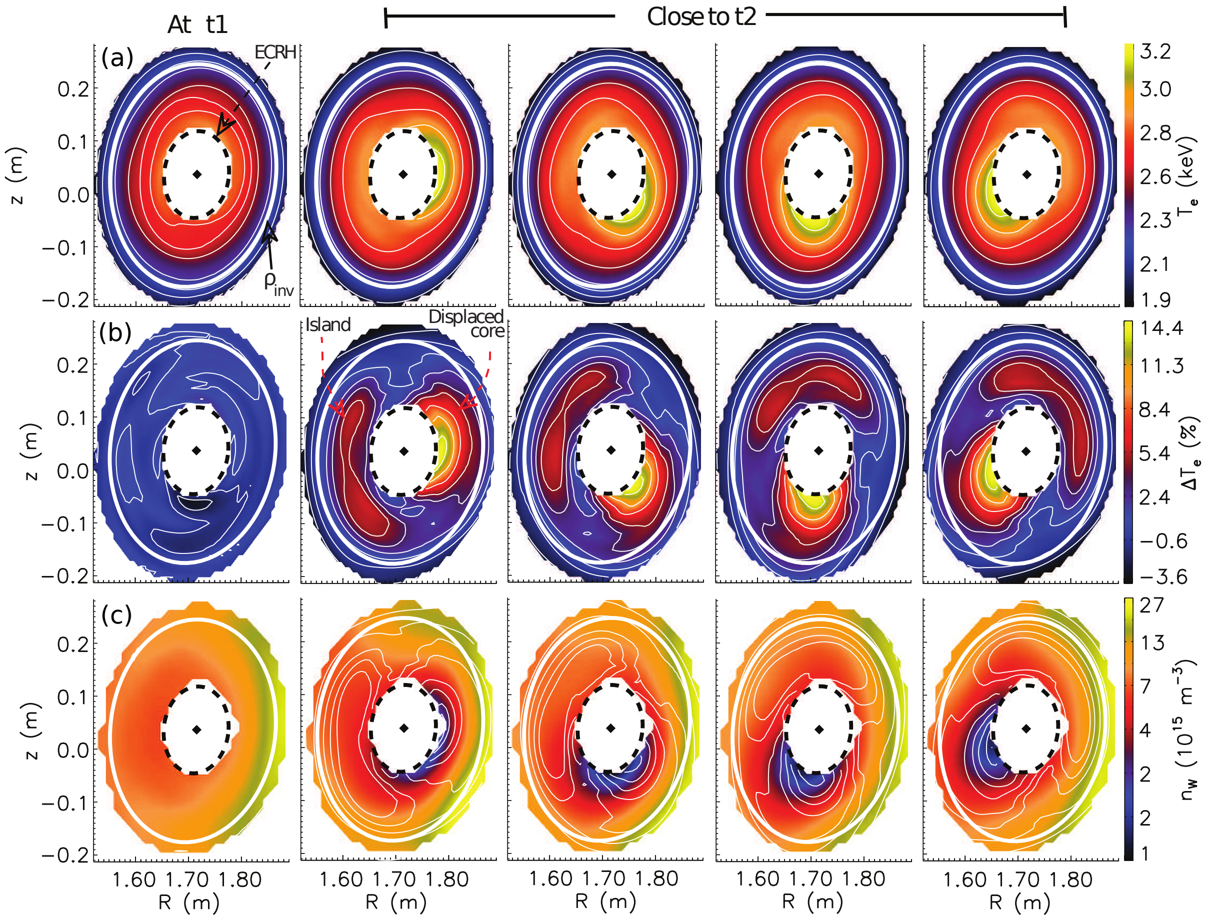

Figure 3: 2D maps: (a) T_e evolution, (b) T_e evolution with respect to the start of the sawtooth cycle ($\sim t_1$); (c) n_W^{SXR} (shaded surface) with the contours of (b) over-plotted for correlation with the mode structure.

The central white area is a region of plasma not covered by the ECE diagnostic and therefore not accounted for in the 2D analysis. Figure 3b shows the percentage change in T_e with respect to the start of the sawtooth cycle ($\Delta T_e(t) = (T_e(t) - \langle T_e(t_1)\rangle)/\langle T_e(t_1)\rangle$). From the isothermal contours of both figures 3a and 3b the rotating displaced core is clearly distinguishable, figure 3b clearly shows the mode structure, with the displaced core and the magnetic island (see labels) rotating in the laboratory frame in the clockwise direction. The 2D W density (figure 3c) inside the inversion radius is relatively flat at the start of the cycle, exhibiting a slight poloidal asymmetry consistent with LFS accumulation due to centrifugal effects. This asymmetry is visible during mode saturation close to the inversion radius, while inside ρ_{inv} the W density is hollow. This *impurity hole*, already visible in the 1D profiles (figure 2), is located inside the displaced core and rotates with it. The magnetic island exhibits instead a flat W density in all mode phases. Comparing the last of these 2D W density plots (figure 4c) with the modelling from GKW+NEO (figure 4a), while, as already clear from the 1D profiles (figure 2f), the hollowness inside the inversion radius is not reproduced, the poloidal asymmetry around and outside of ρ_{inv} is very well matched.

It is thus clear that modelling in 3D is required to account for the helically displaced core of the $(1,1)$ mode as well as the presence of the magnetic island. Neoclassical, turbulent and MHD simulations investigating the transport of W in a non-axisymmetric AUG geometry in the presence of an ideal $(1,1)$ mode are ongoing using the code EUTERPE [9, 10], GENE [11] and XTOR-2F [12, 13] respectively. Due to the stellarator-like equilibrium arising in the presence of the saturated $(1,1)$ mode (effective magnetic field ripple ε_{eff} of the order of what encountered in LHD and higher than what expected for W7X, figure 4c), the effects of the non-axisymmetry are expected to be present also outside the $q = 1$ surface where complete axisymmetry is still not recovered ($\varepsilon_{eff} > 0$) [10].

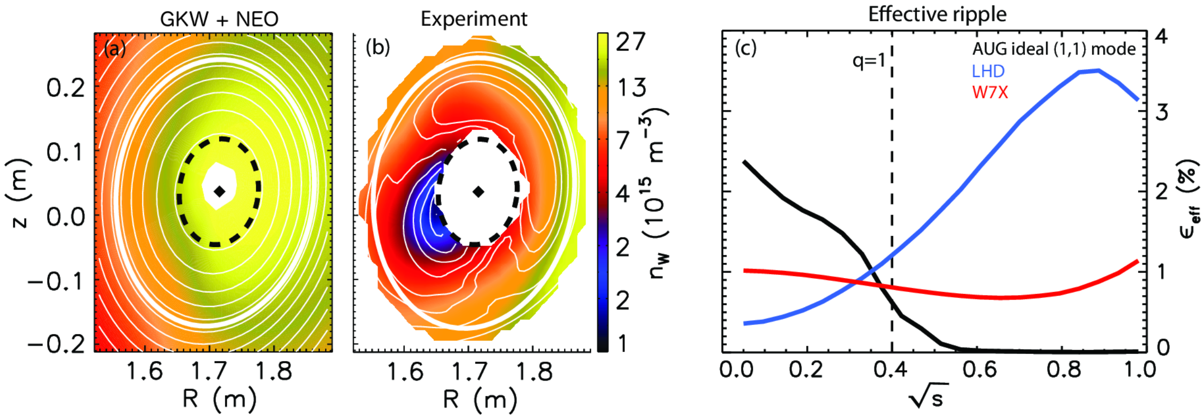

Figure 4: 2D W density maps from GKW+NEO (a) and experiment (b). Effective ripple of AUG discharge #31114 with ideal internal kink ($\xi \sim 10$ cm) compared to standard LHD and W7X configurations (c) [10]. The coordinate $\sqrt{s}$ corresponds to the normalised toroidal flux.

Acknowledgments: This work has been carried out within the framework of the EUROfusion Consortium and has received funding from the Euratom research and training programme 2014-2018 under grant agreement No 633053. The views and opinions expressed herein do not necessarily reflect those of the European Commission.

References: **[1]** M. Odstrcil et al., Nucl. Instr. and Methods in Phys. Research A **686**, 156 (2012), **[2]** M. Sertoli et al., Nucl. Fusion **53**, 053015 (2013), **[3]** A. Peeters et al., Comp. Phys. Comm. **180**(12), 2650 (2009), **[4]** E. A. Belli et al., Plasma Phys. Control. Fusion **54**(1), 015015 (2012), **[5]** C. Angioni et al., Nucl. Fusion **54**(8), 083028 (2014), **[6]** M. Sertoli et al., Plasma Phys. Control. Fusion **57**(7), 075004 (2015), **[7]** M. Sertoli et al., Submitted to Nucl. Fusion, **[8]** A. Gude et al., 37th EPS Conference, P4.124 (2010), **[9]** G. Jost et al., Phys. Plasmas **8**(7) (2001), **[10]** J. Garcia-Regaña, This conference, P2.170, **[11]** F. Jenko et al., Phys. Plasmas **7** (2000) 1904, **[12]** H. Lütjens et al., J. Comput. Phys. **229**(21), 8130 (2010), **[13]** J. Ahn, This conference, P1.103